International Research Journal of Innovations in Engineering and Technology (IRJIET)

ISSN (online): 2581-3048
Volume 6, Issue 2, pp 42-53, February-2022
https://doi.org/10.47001/IRJIET/2022.602009

Laboratory Investigation of the Physico-Mechanical Properties of Coral Limestone of Vipingo Area in Kenya's Coastal Region

[1]Joan Atieno Onyango, [2]Dorothy Mwanzia Kanini, [3]Dyson Moses, [4]Cho Thae Oo, [5]Ulaankhuu Batsaikhan, [6]Seelae Phaisopha, [7]Ian Tsuma Krop

[1,7]Department of Mining, Materials and Petroleum Engineering, Jomo Kenyatta University of Agriculture and Technology, P.O. Box 62000-00200, Nairobi, Kenya
[2]Department of Physics, Jomo Kenyatta University of Agriculture and Technology, P.O. Box 62000-00200, Nairobi, Kenya
[3]Department of Geography and Earth Sciences, School of Applied Science, University of Malawi, P.O Box 280, Zomba, Malawi
[4,5,6]Department of Earth Resources Engineering, Faculty of Engineering, Kyushu University, Fukuoka 819-0395, Japan

***Abstract* - This study investigates physical and mechanical characteristics of the Pleistocene coral limestone of Kenya's coastal plain by laboratory experiments based on ASTM standards. The experiments have done include uniaxial compression test, indirect tensile test, ultrasonic pulse velocity (UPV) test, saturation porosity for porosity and direct shear test. Engineering properties of brittleness, Schmidt's rebound number, fracture index and drillability index are calculated from empirical equations based on the tensile strength and uniaxial compressive strength available in published literature. The various moduli are also calculated from equations based on the P-wave and S-wave velocities from UPV test. The average values of the investigated physical properties include bulk density (2199kg/m^3), porosity (8.47%). The average investigated mechanical properties values include uniaxial compressive strength (16.41MPa), tensile strength (1.61MPa), Elastic modulus(31.62GPa), cohesion(133.33kPa) and friction angle (410). The P-wave and S-wave velocities are 4797m/s and 2288m/s respectively. The results presented in this work highlight the influence of rock porosity as an inherent structural feature that affects intact rock properties. The results are discussed with a focus on the variation of properties with porosity, with the conclusion that empirical relationships developed for porous rock should include porosity as a parameter which contributes to variations in rock properties. This paper presents the first published geomechanical data of coral limestone from the reef coral rock formation making up Kenya's coastline.**

Keywords: coral limestone, intact rock, laboratory tests, porosity, weak rock.

I. INTRODUCTION

Geotechnical engineering requires a strong database of rock engineering properties which are crucial input parameters for mining and civil engineering applications. These properties are often determined through in-situ and laboratory methods. However, sometimes it is not possible to experimentally obtain all the required properties given the fact that the procedures for measuring rock properties are expensive and time consuming. Besides that, owing to the discontinuous nature of rock masses, it is sometimes not possible to get sufficient samples for laboratory experiments. Over time, straightforward empirical or theoretical correlations have been obtained between engineering properties such as strength and hardness making it possible to reasonably estimate other rock material properties [1]. With the advent of computer software such as Rocscience'sRocData and RocLab, the work of estimating rock properties has been made even easier but availability or tried and tested data goes a long way in verification to strengthen the empirical formulas and improve on accuracy of the software.

Laboratory testing, when possible, offers a database of important engineering data useful for input into engineering analysis processes, and also as verification data in further theoretical research work. Laboratory testing methods for rocks are based on the American Society for Testing and Materials (ASTM) and International Society of Rock Mechanics (ISRM) standards. Wave velocity is closely related to rock properties and has been used as one of the most important strength index properties[2]. Three non-destructive laboratory methods are available for determining the velocity of elastic waves in a rock namely; the high frequency ultrasonic pulse technique, the low frequency ultrasonic pulse technique and the resonant method[3]. Strength properties such as compression, tensile and shear strength of rock are measured by destructive tests.

Planning in rock engineering operations such as mining and quarrying makes use of engineering properties of rocks such as brittleness (B), hardness (Schmidt's Rebound Number,

International Research Journal of Innovations in Engineering and Technology (IRJIET)

ISSN (online): 2581-3048

Volume 6, Issue 2, pp 42-53, February-2022

https://doi.org/10.47001/IRJIET/2022.602009

RN), fracture toughness (FT) and drillability index (DI). Brittleness can be defined as a physical property of rocks that fracture without plastic flow, being a measure of rock mechanical strength that controls the ease with which cracks can propagate through the rocks [[4], [5]]. The property of hardness refers to the rock material's resistance to permanent deformation from an applied force[6], given by Schmidt's Rebound Number (RN). Kahraman et al.[7]defined fracture toughness (FT) as the rock's resistance to fracture and propagation of pre-existing fractures. Drillability index refers to the ratio of applied force to penetration rate, a property essential in selecting the bit type, average penetration rate as well as approximate bit life[8]. Previous research has shown a strong correlation between strength properties of rock and the aforementioned engineering properties. Hucka& Das [9] for instance established a relationship between UCS(σ_C), tensile strength (σ_T) and brittleness (B) as given by equation (2).

$$\sigma_T = \sigma_C/10 \qquad (1)$$

Brittleness: $B = (\sigma_C * \sigma_T)/2 \qquad (2)$

Altindag [10] further showed that brittleness is useful in calculating the other engineering properties using the equations below;

Schmidt's rebound number:

$$RN = 5.9528 * \ln(B) + 20.933 \qquad (3)$$

Fracture toughness: $FT = 0.11 * (B)^{0.43} \qquad (4)$

Drillability Index:

$$DI = 0.6344 * (B)^{0.6186} \text{ for conical bit} \qquad (5)$$

This work is motivated by some ongoing research work on Vipingo coral limestone quarry in Kenya's coastal region where laboratory tests have been done to obtain input parameters for the analyses. Due to the variability of rock masses, it is important to have data from the actual site under study. In view of the various mined land rehabilitation regulations being implemented, this data will go a long way in guiding closure operations in various quarries in similar geological conditions. Publishing the laboratory results is an immense contribution to the database of rock material properties, especially weak rocks. Laboratory tests in this work are conducted using ASTM standards. Uniaxial compression test, Brazillian test, porosity test, Pulse Velocity test and direct shear are the experiments conducted in this work. The data from the experiments are used together with empirical relationships to determine engineering properties of brittleness, hardness, fracture and drillability index which are also very important parameters in planning quarry operations. Rock porosity is a major contributing to variability of intact rock strength therefore the relationship obtained between various rock properties and porosity is investigated. An outline of the workflow process in this study is as shown in the flow chart in **Figure 1**.

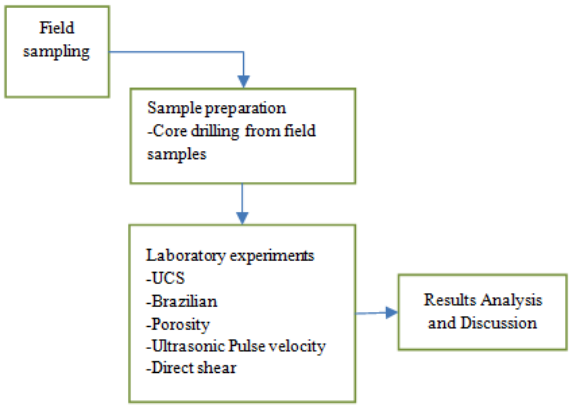

Figure 1: Flow chart

II. AREA UNDER STUDY

2.1 Geographical setting

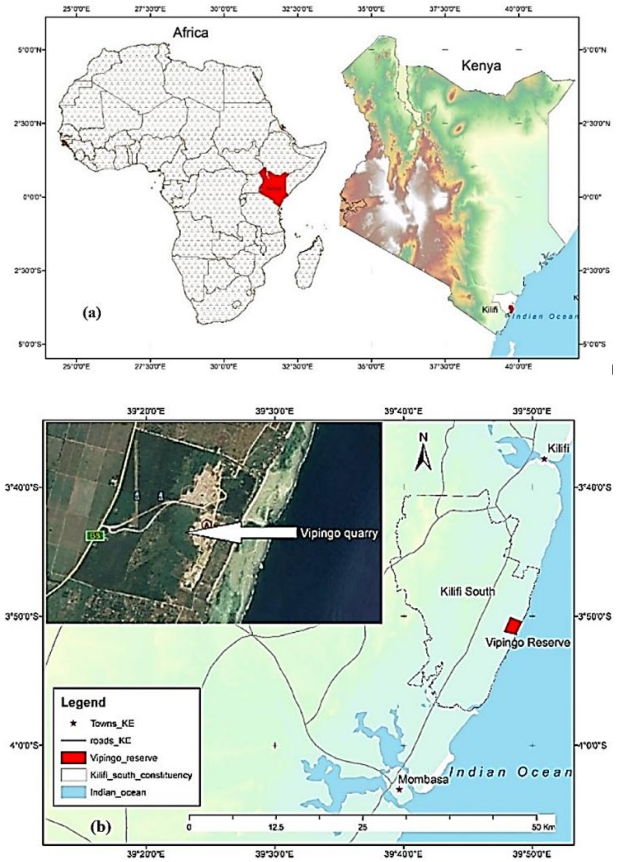

Figure 2: Location of Vipingo Coral Limestone Quarry

Vipingo Coral Limestone Quarry is situated in south-east Kenya in the coastal county of Kilifi **Figure 2(a)** which lies between latitude 2 0'and 4 0'South, and between longitude 39

International Research Journal of Innovations in Engineering and Technology (IRJIET)

ISSN (online): 2581-3048

Volume 6, Issue 2, pp 42-53, February-2022

https://doi.org/10.47001/IRJIET/2022.602009

05'and 40 14'East. The quarry itself falls between latitudes 30 50' 03" and 30 51' 27" South, and longitudes 390 47' 47" and 390 49' 18" parallel to the shoreline of the Indian ocean **Figure 2(b).** Limestone deposits extend approximately 180k N-S along the coastal zone from the Tanzania border to the Malindi area, the resource forming a 4-8km wide band about 70m thick running parallel to the coast.

2.2 Geology of the area

The Vipingo coralline rock mass formation is of the Pleistocene age. Structurally, there is no distinct bedding or foliation is visible in this rock formation, and joints are not quite well defined. It is visibly highly porous and the total carbonates content is about 95%. As a consequence of the normal reef building mechanisms which results in high porosity, there is high content of entrapped silica, which together the aeolian free sands increase the variability of the grade of the limestone. Karstification is evident in some well-defined sections resulting in distinct voiding and caving. The samples used in this work are collected from Vipingo quarry.

III. METHODS AND TESTING PROCEDURES

3.1 Field Sampling

Figure 3: Sampling locations

The fieldwork involved systematic sampling at various depths from the locations in **Figure 3** in order to get a more inclusive sample representation of the rock type structural features. The rock mass does not have any distinct beddings or foliations, therefore a variation in the depth of sample location was considered key in getting a good representation of the rock properties. Given the highly porous nature of the rock mass as can be seen in **Figure 4,** it was not possible to obtain drill core samples that could be used in the tests. The rock blocks in **Figure 5** were therefore collected at various locations considering the target laboratory test sample dimensions.

Figure 4: Drill core with very low recovery

Figure 5: Samples at the field

3.2 Sample preparation

The samples were prepared in accordance with ASTM standards as stipulated in ASTM D4543-08[10]. The process involved here is core drilling using rock coring equipment to obtain cylindrical core samples (**Figure 7**) from the irregularly shaped field samples as can be seen in **Figure 6(a)&(b)**, then grinding to flatten the ends as shown in **Figure 6(c)**.

International Research Journal of Innovations in Engineering and Technology (IRJIET)

ISSN (online): 2581-3048

Volume 6, Issue 2, pp 42-53, February-2022

https://doi.org/10.47001/IRJIET/2022.602009

(a) Core drilling (b) Core drilling (c) Grinding to size

Figure 6: Rock coring

Figure 7: Ready cylindrical samples

3.3 Testing Procedures and Results

All test procedures are in accordance with ASTM standards. The samples are identified using the field sample labeling for purposes of traceability.

3.3.1 Chemical Composition

An XRF analysis conducted gives the chemical composition of Vipingo coral limestone as shown in **Table 1** below.

Table 1: Chemical composition of coral limestone rock

Chemical	% Composition
Cao	33.21-54.94
SiO_2	0.85-36.93
Al_2O_3	0.80-4.98
Fe_2O_3	0.18-4.14
MgO	0.32-0.88
Na_2O	0-0.14
K_2O	0.02-0.63
SO_3	0.03-12.97
P_2O_5	0.03-0.06
Mn_2O_3	0-0.09
TiO_2	0.04-0.31

Table 2: Porosity test results

S/N.	1	2	3	4	5	6	7	8	9	10
Field Sample	3	12	14	21	22	1	8	10	16	48
Porosity (%)	10.70	1.56	11.82	5.40	13.15	6.47	6.65	14.97	6.17	7.77

3.3.2 Porosity Test

Porosity of the samples was done by saturation method where the specimen is saturated by water immersion in a vacuum of less than 800Pa for a period of at least 1 hour. The experimental setup showing sample saturation and oven drying are shown in **Figure 8**. The specimen is then removed and surface dried using a moist cloth after which the saturated mass M_{sat} is determined. The specimen's dry mass Ms is taken after drying it to a constant mass at a temperature of 105°C and allowing it to cool off for 30min. The specimen bulk volume V is calculated from caliper readings for each dimension. The rock porosity is then calculated using equation (7), which whose parameters are determined by equation (6). The porosity tests result from 10 samples are summarized in **Table 2**.

$$\text{Pore volume, } V_v = \frac{M_{sat} - M_s}{\rho_w} \qquad (6)$$

$$\text{Porosity, } n = \frac{100 V_v}{V}\% \qquad (7)$$

Where

ρ_w =density of water

V-specimen bulk volume

Msat=specimen's saturated mass

Ms=specimen's dry mass

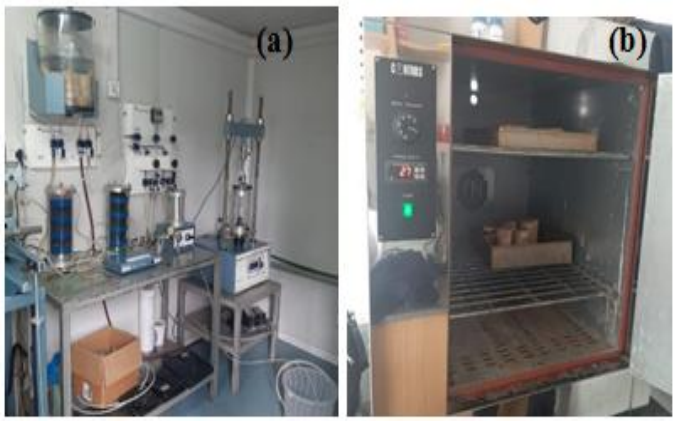

a) The saturation process b) Oven drying

Figure 8: Porosity test set-up

International Research Journal of Innovations in Engineering and Technology (IRJIET)

ISSN (online): 2581-3048

Volume 6, Issue 2, pp 42-53, February-2022

https://doi.org/10.47001/IRJIET/2022.602009

3.3.3 Ultrasonic Pulse Velocity (UPV) test

The UPV test is for determination of Poisson's ratio and the Modulus of Elasticity by measuring with P-wave (Vp) and S-wave (Vs) transducers. The test procedure involves applying shear wave coupling gel on the transducers and pressing them firmly on either ends of the specimen while connected to Pundit Lab. 250 kHz shear wave transducer is used in the experimental setup shown in Figure 9 and Figure 10 shows the readings from Pundit Lab.

By measuring a P-wave transmission time and an S-wave transmission time with Pundit Lab, the P-wave modulus (M).

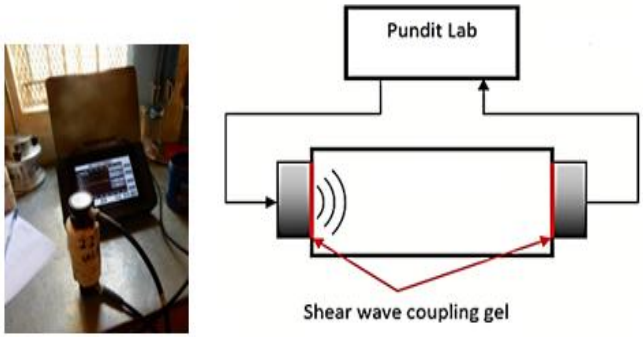

Figure 9: Performing measurements with the 250 kHz shear wave transducers

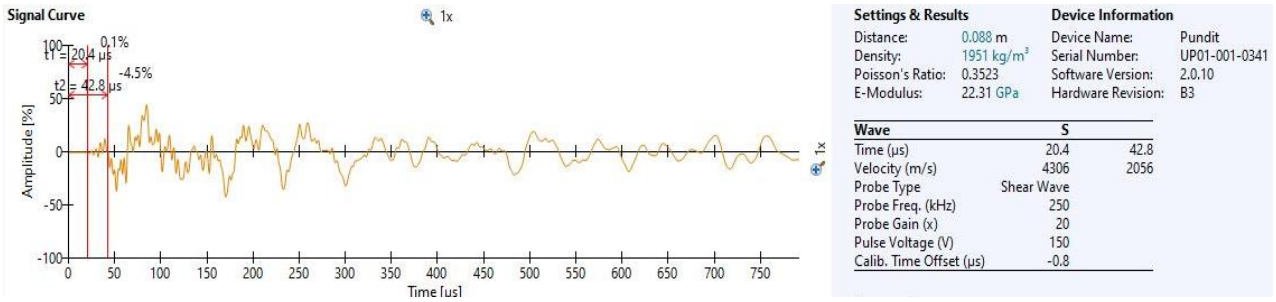

Figure 10: Plot from Pundit Lab

And the Shear modulus (G) using equation (9) and equation (10) respectively. The velocity is computed using equation (8);

$$V = \frac{\text{Length of sample}}{\text{Travel time}} \text{X } 10e6 \text{ m/s} \qquad (8)$$

P-wave modulus (M):

$$M = \rho V_p^2 \qquad (9)$$

Where ρ is the density of the material and V_p is the pulse velocity of the P-wave.

Shear-modulus (G):

$$G = \rho V_s^2 \qquad (10)$$

Where ρ is the density of the material and Vs is the pulse velocity of the S-wave.

Using the equations above we can determine Poisson's ratio (ν) as illustrated in equation (11):

$$\nu = \frac{M-2G}{2M-2G} = \frac{\rho V_p^2 - 2\rho V_s^2}{2\rho V_p^2 - 2\rho V_s^2} = \frac{V_p^2 - 2V_s^2}{2V_p^2 - 2V_s^2} = \frac{V_p^2 - 2V_s^2}{2(V_p^2 - V_s^2)} \qquad (11)$$

The Poisson's ratio can therefore be determined simply by measuring the P-wave velocity and the S-wave velocity without necessarily knowing the density of the material. After determining the Poisson's ratio, the elastic modulus can then be calculated from equation (12), in which case it is necessary to know the density of the material.

$$E = 2G(1+\nu) \qquad (12)$$

The results obtained from UPV test are detailed in **Table 3** and **Table 4**.

Table 3: Ultrasonic test results

S/N.	Sample	Sample Length (mm)	Porosity (%)	P-Wave Transmission Time (µs)	P-Wave velocity (m/s)	S-Wave Transmission Time (µs)	S-Wave velocity (m/s)	Poisson's Ratio
Dry Samples								
1.	3	87.70	10.70	20.4	4306	42.8	2056	0.35
2.	12	97.20	1.56	17.7	5491	38.0	2550	0.36
3.	14	95.80	11.82	22.7	4230	45.9	2093	0.34
4.	21	98.20	5.40	17.8	5502	35.7	2743	0.33
5.	22	93.50	13.15	19.6	4789	47.0	1999	0.39

International Research Journal of Innovations in Engineering and Technology (IRJIET)
ISSN (online): 2581-3048
Volume 6, Issue 2, pp 42-53, February-2022
https://doi.org/10.47001/IRJIET/2022.602009

Saturated Samples								
6.	9	49.00	8.43	18.1	5639	44.1	2310	0.40
7.	11	47.70	3.76	16.7	5758	39.2	2448	0.39
8.	17	49.00	17.20	43.2	2476	91.0	1175	0.35
9.	44	49.20	5.31	18.9	5647	39.9	2679	0.35
10.	50	51.90	15.25	22.8	4127	47.7	1971	0.35

Table 4: Moduli derived from the wave velocities

S/N.	Elastic Modulus, E(GPa)	Bulk Modulus, K(GPa)	Shear Modulus, G(GPa)	P-wave Modulus, M(GPa)
Dry Samples				
1.	22.31	2.20	8.25	36.18
2.	44.53	4.08	16.35	75.79
3.	24.45	2.64	9.14	37.33
4.	45.73	5.04	17.13	68.92
5.	21.08	1.48	7.56	43.39
Saturated Samples				
6.	35.91	2.42	12.46	74.25
7.	38.91	2.86	14.94	82.66
8.	7.13	0.69	2.63	11.68
9.	41.54	4.02	17.26	76.67
10.	26.20	2.58	8.3	36.39

3.3.4 Unconfined Compression Test (Dry Samples)

UCS test was based on ASTM D2938 standards [11] using the ASTM C39 compression test machine **(Figure 11)**. Axial load was applied at a rate of 1MPa/s till failure. The rock density was auto-generated during the UCS test. The samples had a length to diameter ratio of 2:1. Bulk density of the samples was obtained automatically from the UCS machine. The compressive strength in the test specimen is calculated from the maximum compressive load on the specimen and the initial computed cross-sectional area using equation (13). **Table 5** details the results of uniaxial compression test.

$$\sigma = \frac{P}{A} \qquad (13)$$

Where:

σ = Compressive strength
P= Maximum load
A = Cross sectional area.

(a) Uniaxial compression machine

b) Before compression

(c) Post failure

Figure 11: Uniaxial Tensile Test set-up

International Research Journal of Innovations in Engineering and Technology (IRJIET)
ISSN (online): 2581-3048
Volume 6, Issue 2, pp 42-53, February-2022
https://doi.org/10.47001/IRJIET/2022.602009

Table 5: Uniaxial Compression test results

S/N.	Sample No.	Diameter (mm)	Length (mm)	Density (Kg/m^3)	Failure Load(kN)	UCS (MPa)	Porosity (%)	Failure mode
1.	3	54.00	87.70	1951	12.0	5.24	10.70	Multiple Fracturing
2.	12	55.00	97.20	2514	41.9	17.64	1.56	Axial Splitting
3.	14	54.80	95.80	2086	41.1	17.43	11.82	Axial Splitting
4.	14	55.20	98.20	2277	86.3	36.06	5.40	Axial Splitting
5.	21	54.70	93.50	1892	13.4	5.70	13.15	Multiple Fracturing

3.3.5 Tensile Test

Tensile strength was determined by the splitting/Brazillian test in accordance with ASTM D3967 standards [12]. In the Brazilian test, a disc shape specimen of the rock is loaded by two opposing normal strip loads at the disc periphery (**Figure 12**). The thickness/diameter ratio of the specimen was in the range of 0.5 to 0.6. At failure, the tensile strength of the rock is calculated using equation (14). The results of the indirect tensile test are tabulated in **Table 6**.

$$\sigma_t = \frac{2P}{\pi LD} \qquad (14)$$

Where:

σ_t= splitting tensile strength, MPa

P = maximum applied load indicated by the testing machine, N

L = thickness of the specimen, mm

D = diameter of the specimen, mm

(a) Before failure **(b) Post failure**

Figure 12: Brazilian test setup

3.3.6 Direct Shear Test

This is a test carried out to determine the shear strength properties of the rock i.e. the angle of internal friction and cohesion. The test was conducted in accordance to ASTM D5607-02 guidelines [13]. The experimental apparatus is as shown in **Figure 13**. The specimen is encapsulated in concrete as shown in **Figure 13(a)**. The applied normal loads and corresponding shear loads are recorded and plotted on the Mohr-Coulomb stress plot to obtain the cohesion from the y-intercept and friction angle from the slope angle of the fitted curve. A plot of shear versus normal stress that gives the values of cohesion and friction angle is given in **Figure 14.**

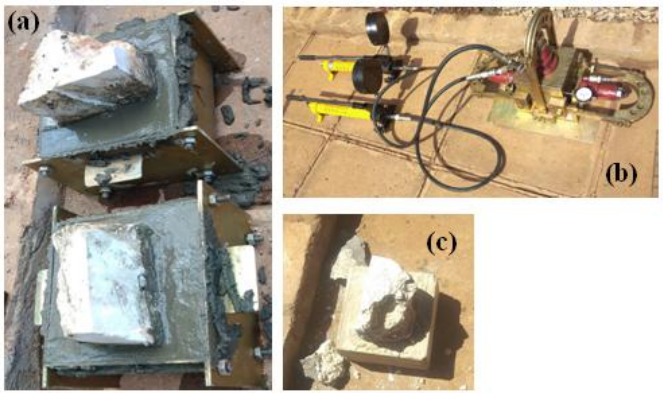

a) Sample preparation b) The loading device c) The sheared rock

Figure 13: Direct shear test

Specimen Test Stage	*Density kg/m³	Vertical Stress mpa	Shear Stress mpa	Regression Line mpa
1	2324	25.00	22.00	21.9
2	2463	30.00	26.00	26.2
3	2238	35.00	30.70	30.6

Phi (Φ):- 41 13 kPa

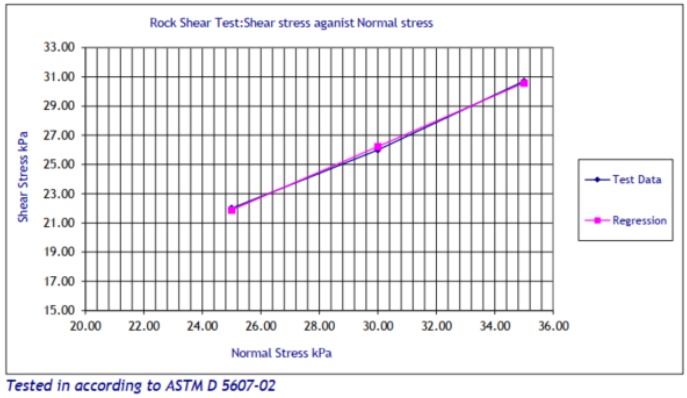

Tested in according to ASTM D 5607-02

Figure 14: Direct shear test result

3.3.7 Calculated Engineering properties

The engineering properties previously introduced in section 1.0 are calculated from the formulas in equations 1 to 5 and tabulated in **Table 6.**

International Research Journal of Innovations in Engineering and Technology (IRJIET)

ISSN (online): 2581-3048

Volume 6, Issue 2, pp 42-53, February-2022

https://doi.org/10.47001/IRJIET/2022.602009

Table 6: Engineering properties

Sample No.	Porosity (%)	UCS (MPa)	TS (MPa)	B	RN	FT (MPa.m$^{1/2}$)	DI (kN/mm)
3	1.56	17.64	1.76	15.56	37.27	0.36	3.47
12	5.40	36.06	3.61	65.02	45.78	0.66	8.39
14	10.70	5.24	0.52	1.37	22.82	0.13	0.77
14	11.82	17.43	1.74	15.19	37.13	0.35	3.41
21	13.15	5.70	0.57	1.62	23.82	0.14	0.86
1	6.17	15.46	1.55	11.95	35.70	0.32	2.94
8	6.47	22.37	2.24	25.02	40.10	0.44	4.65
10	6.65	10.57	1.06	5.58	31.17	0.23	1.84
16	7.77	20.67	2.07	21.36	39.16	0.41	4.22
48	14.97	11.35	1.14	6.44	32.02	0.25	2.01

KEY: TS: Tensile Strength B: Brittleness; RN: Schmidt's Rebound Number; FT: Fracture Toughness; DI: Drillability Index;

IV. DISCUSSION

One characteristic feature of coral limestone is its porosity. The discussion revolves around rock porosity as an inherent structural feature that controls the behavior of the rock. The structure of the specimens as seen in **Figure 7** vary from small pores to large ones which make it a bit difficult to obtain the desired sizes of intact cores, and grinding the core ends flat is an added challenge.

4.1 Bulk Density

The bulk density of the rock varies with porosity as shown in **Figure 15**. The trend is clear reduction of rock density with increasing porosity as a consequence of reduced solid mass from voiding. This phenomenon is congruent with results obtained by Xu et al. [14], Yasar & Erdogan [15] and Chang et al. [16] among other researchers who have investigated rock properties.

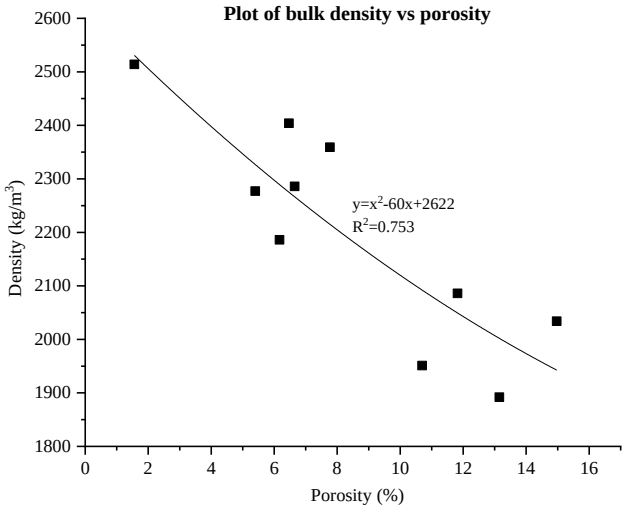

Figure 15: Graph of variation of bulk density with rock porosity

4.2 The P-wave and S-wave velocities

The wave velocities decrease with increasing porosity. The P-wave velocity is seen to be higher in saturated samples than in dry samples **(Figure 16)**. In the case of S-wave velocity, the values are higher for dry samples when the porosity is below 7% **(Figure 17)**. At higher porosity values the S-wave velocity is higher in saturated samples. This phenomenon is similar with results from experiments done on sandstones by Kassab & Weller [17].

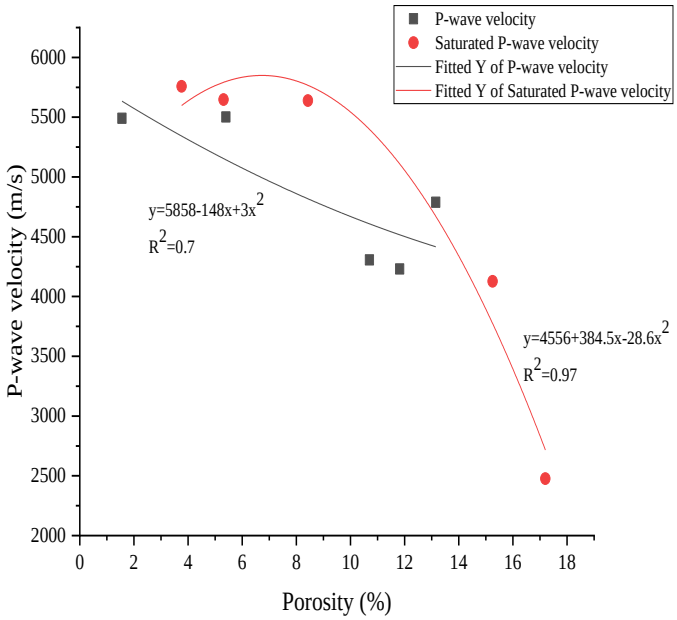

Figure 16: Variation of P-wave velocity with rock porosity

International Research Journal of Innovations in Engineering and Technology (IRJIET)

ISSN (online): 2581-3048

Volume 6, Issue 2, pp 42-53, February-2022

https://doi.org/10.47001/IRJIET/2022.602009

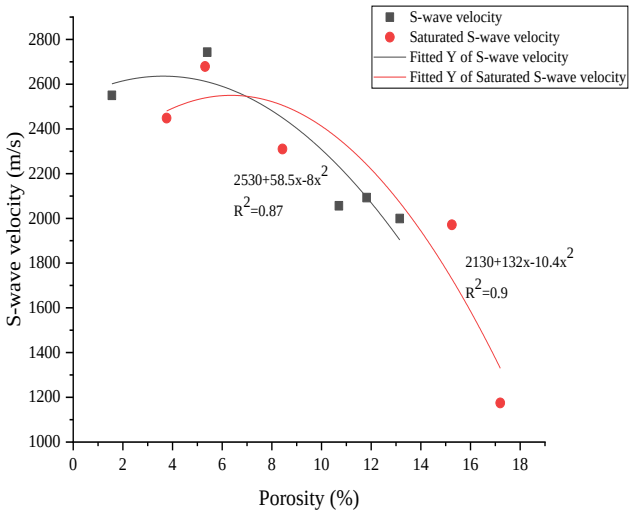

Figure 17: Variation of S-wave velocity with rock porosity

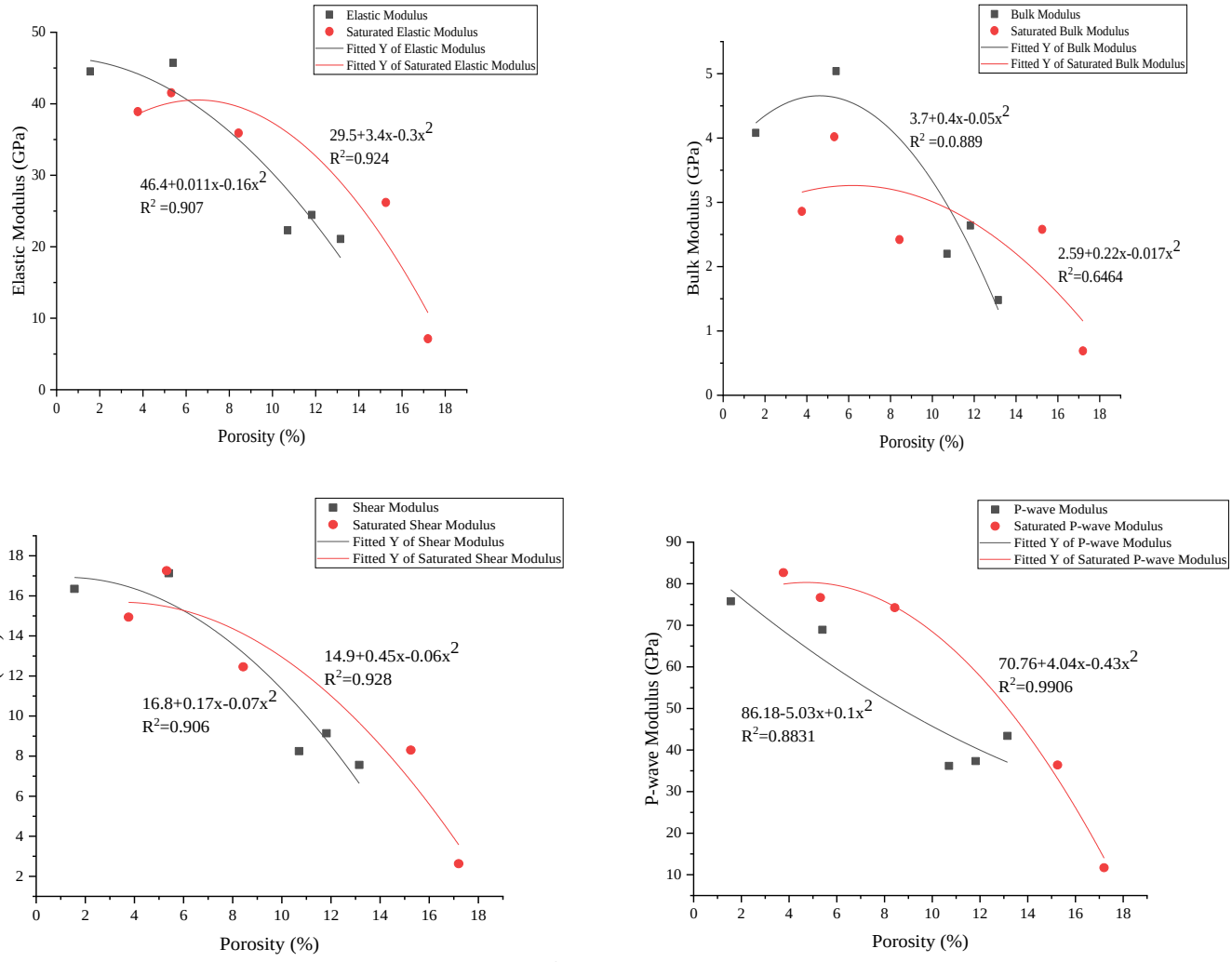

Figure 18: Variation of various moduli with rock porosity

The various moduli of the rock are also observed to reduce with increasing porosity as depicted by the graphs in **Figure 18**, similar phenomenon to the case of the wave velocities which were used to calculate the moduli.

4.3 Uniaxial compression and Tensile strengths

It was observed that in uniaxial compression test, the more intact cores with lower porosity experience axial splitting **(Figure 11)** while multiple fracturing is characteristic of

International Research Journal of Innovations in Engineering and Technology (IRJIET)

ISSN (online): 2581-3048

Volume 6, Issue 2, pp 42-53, February-2022

https://doi.org/10.47001/IRJIET/2022.602009

higher porosities. This means the distribution and dimensions of pores in the rock structure have a direct bearing on the mode of failure. The data points obtained were however insufficient for developing any meaningful correlation between the compression and tensile strengths versus porosity. Even so, a trend can be observed in **Figure 19** of reducing intact rock strength with increasing porosity, consistent with experimental results done on sandstone by Eremin[18] and Price et al. [19].

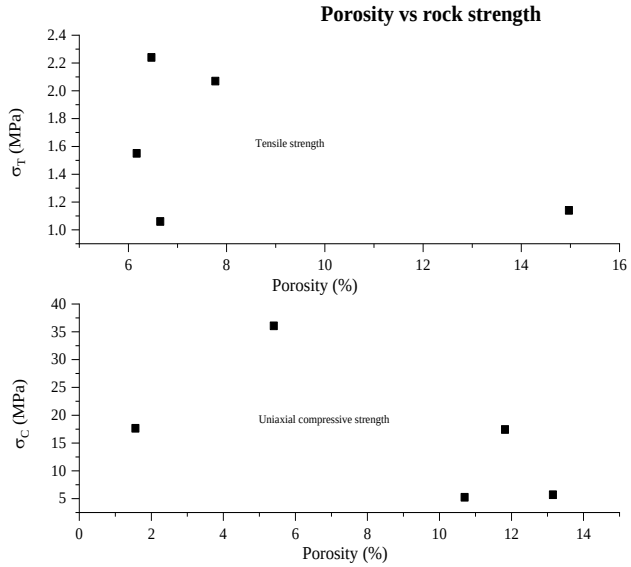

Figure 19: Graph of variation of rock strength with porosity

4.4 Cohesion and Friction Angle

The Mohr-Coulomb failure envelope in **Figure 20** was plotted using direct shear test results in **Figure 14**. The shear strength properties of the rock present a case of low cohesion (133.33kPa) and high friction angle (41^0). According to Wyllie & Norrish [20], this phenomenon is as a result of the roughness of the sliding surface.

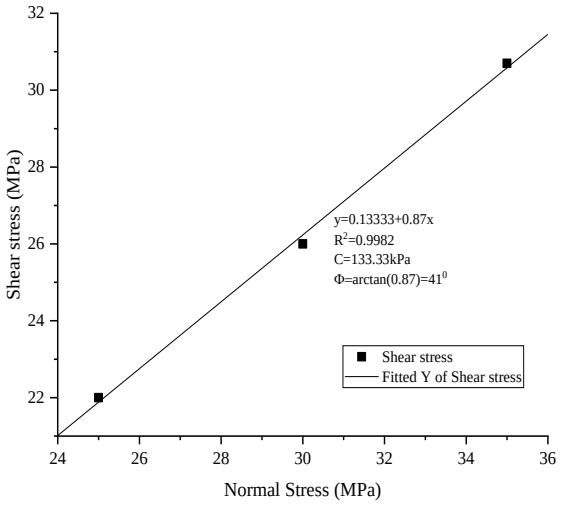

Figure 20: Linear Mohr-coulomb failure envelope

4.5 The Engineering Properties

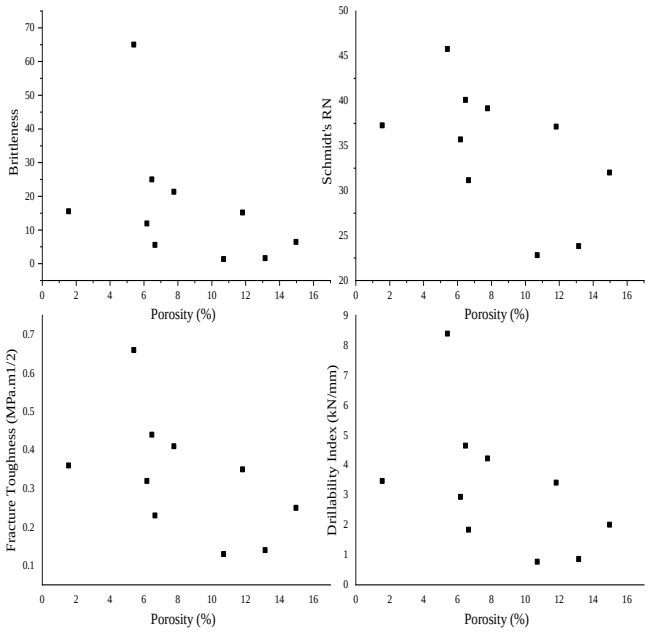

Figure 21: Variation of engineering properties with porosity

4.6 Summary of the rock properties

Equation (1) states that the tensile strength is a tenth of the uniaxial compressive strength. The results in Table 8 also show that the average is a tenth of the UCS. This basic correlation which agrees with previous research gives confidence on the other engineering properties calculated using the two values. **Figure 21** gives an impression of the variation of the engineering properties of rock with porosity. Due to a wide scatter of the few data points, no empirical relationship was obtained. However, with more data points, it is possible to obtain a better relationship between the engineering properties and rock porosity. In this regard, it can be possible to develop the empirical equations further to include and quantify the impact of rock porosity and as a factor that affects the behavior of rock.

The average phyico-mechanical properties of the rock obtained from the laboratory experiments detailed above are summarized in Table 8. ISRM classifies rocks depending their compressive strength, from weak to medium strength to strong rocks. Out of the five samples tested, only one had UCS value above 25 and the average value of UCS is 16.41MPa. The rock can therefore be classified as weak based on the ISRM classification scheme in **Figure 22**.

International Research Journal of Innovations in Engineering and Technology (IRJIET)

ISSN (online): 2581-3048

Volume 6, Issue 2, pp 42-53, February-2022

https://doi.org/10.47001/IRJIET/2022.602009

Table 8: Summary of the rock properties

Property	Symbol	Units	Range	Average
Bulk density	ρ	(kg/m^3)	1892-2514	2199
Porosity	n	%	1.56-14.97	8.47
Poisson's ratio	ν		0.33-0.4	0.36
P-wave velocity	V_p	m/s	4230-5502	4797
S-wave velocity	V_s	m/s	1999-2743	2288
P-wave velocity(saturated)	V_p	m/s	2476-5758	4729
S-wave velocity(saturated)	V_s	m/s	1175-2679	2117
Uniaxial Compressive Strength	σ_C	MPa	5024-36.06	16.41
Tensile strength	σ_T	MPa	1.06-2.24	1.61
Cohesion	C	kPa	133.33	133.33
Friction angle	ϕ	(^{0})	41	41
Elastic modulus	E	GPa	21.08-45.73	31.62
Shear modulus	G	GPa	7.56-17.13	11.69
Bulk modulus	K	GPa	1.48-5.04	3.09
P-wave modulus	M	GPa	36.18-75.79	52.32
Brittleness	B		1.37-65.02	16.91
Schmidt's rebound number	RN		22.82-45.78	34.50
Fracture toughness	FT	$MPa.m^{1/2}$	0.13-0.66	0.33
Drillability Index	DI	kN/mm	0.77-8.39	3.26

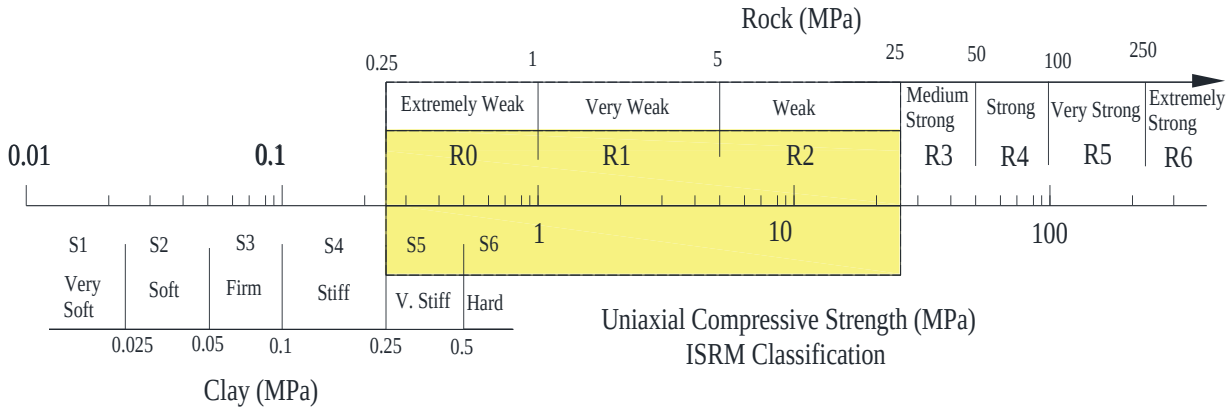

Figure 22: ISRM classification of rock [21]

V. CONCLUSIONS

This paper has compiled laboratory testing data on the geomechanical properties of coral limestone from Kenya's coast. The work looked into variation of rock properties with porosity and the results are consistent with research on other porous rocks. From the main results of the study, the sample density, uniaxial compressive strength and tensile strength decrease with increasing porosity. The rock is classified as weak based on ISRM classification. The sample P- and S-wave velocities decrease with increasing porosity, and the same trend is observed for the various moduli obtained. It is clear that porosity is a factor that results in variations of rock properties and therefore empirical relations of rock properties should include porosity parameter. In this work however, the data points were not sufficient to obtain empirical relationships for rock properties against porosity. The data from this study is a good contribution to the database of weak rock geomechanical properties besides offering valuable information for mine planning and design in this type of rock mass. Further work should look into the saturated properties of rock, properties of coral sand and rock with soil filled voids. Due to the challenges in doing laboratory experiments, more work should go into developing simpler numerical models for simulating tests on porous rock.

ACKNOWLEDGEMENT

The authors are very grateful to Vipingo quarry management for availing the samples for the experiments and Goeissa Laboratory for their technical support in carrying out the experiments. The work is done under JICA scholarship.

REFERENCES

[1] J. Szlavin, "Relationships between some physical properties of rock determined by laboratory tests," *Int. J. Rock Mech. Min. Sci.*, vol. 11, no. 2, pp. 57–66, 1974,

ISSN (online): 2581-3048
Volume 6, Issue 2, pp 42-53, February-2022
https://doi.org/10.47001/IRJIET/2022.602009

doi: 10.1016/0148-9062(74)92649-7.

[2] "Lianyang Zhang - Engineering Properties of Rocks-Butterworth-Heinemann (2016).pdf." .

[3] ISRM, "Suggested methods for determining sound velocity," *Int. J. Rock Mech. Min. Sci. Geomech. Abstr.*, vol. 15, no. 2, pp. 53–58, 1978, doi: 10.1016/0148-9062(78)91013-6.

[4] K. B. Chary, L. P. Sarma, K. J. P. Lakshmi, N. A. Vijayakumar, V. N. Lakshmi, and M. V. M. S. Rao, "Evaluation of Engineering Properties of Rock Using Ultrasonic Pulse Velocity and Uniaxial Compressive Strength," *Natl. Semin. Non-Destructive Eval.*, pp. 379–385, 2006.

[5] N. Goktan RM & Gunes Yilmaz, "A new methodology for the analysis of the relationship between rock brittleness index and drag pick cutting efficiency," *J. South. African Inst. Min. Metall.*, vol. 105, no. 10, pp. 727–733, 2005.

[6] E. Ritz, M. M. Honarpour, J. Dvorkin, and W. F. Dula, "Core hardness testing and data integration for unconventionals," 2014.

[7] S. Kahraman, C. Balcı, S. Yazıcı, and N. Bilgin, "Prediction of the penetration rate of rotary blast hole drills using a new drillability index," *Int. J. Rock Mech. Min. Sci.*, vol. 37, no. 5, pp. 729–743, 2000.

[8] Z. W. Wang, "The mechanics of diamond core drilling of rocks." University of Alaska Fairbanks, 1995.

[9] V. Hucka and B. Das, "Brittleness determination of rocks by different methods," in *International Journal of Rock Mechanics and Mining Sciences & Geomechanics Abstracts*, 1974, vol. 11, no. 10, pp. 389–392.

[10] ASTM International, "ASTM Standard D4345 – 85: Practice for Preparing Rock Core Specimens and Determining," *ASTM Int. West Conshohocken, PA, USA.*, vol. 04, pp. 4–7, 2008.

[11] ASTM International, "ASTM Standard D2938 – 95: Standard Test Method for Unconfined Compressive Strength of Intact Rock Core Specimens," *ASTM Int. West Conshohocken, PA, USA.*, vol. 95, no. D2938-95, pp. 1–3, 2002.

[12] ASTM International, "ASTM Standard - D3967-08: Standard test method for splitting tensile strength of intact rock core specimens.," *ASTM Int. West Conshohocken, PA, USA.*, pp. 8–11, 2008, doi: 10.1520/D3967-08.2.

[13] ASTM International, "ASTM Standard D5607 - 02 Standard Test Method for Performing Laboartory Direct Shear Strength Tests of Rock Specimens Under COnstant Normal Force," *ASTM Int. West Conshohocken, PA, USA.*, vol. 04, 2002.

[14] H. Xu *et al.*, "Characterization of Rock Mechanical Properties Using Lab Tests and Numerical Interpretation Model of Well Logs," *Math. Probl. Eng.*, vol. 2016, 2016, doi: 10.1155/2016/5967159.

[15] E. Yasar and Y. Erdogan, "Correlating sound velocity with the density, compressive strength and Young's modulus of carbonate rocks," *Int. J. Rock Mech. Min. Sci.*, vol. 41, no. 5, pp. 871–875, 2004, doi: 10.1016/j.ijrmms.2004.01.012.

[16] C. Chang, M. D. Zoback, and A. Khaksar, "Empirical relations between rock strength and physical properties in sedimentary rocks," *J. Pet. Sci. Eng.*, vol. 51, no. 3–4, pp. 223–237, 2006, doi: 10.1016/j.petrol.2006.01.003.

[17] M. A. Kassab and A. Weller, "Study on P-wave and S-wave velocity in dry and wet sandstones of Tushka region, Egypt," *Egypt. J. Pet.*, vol. 24, no. 1, pp. 1–11, Mar. 2015, doi: 10.1016/J.EJPE.2015.02.001.

[18] M. Eremin, "Influence of the porosity on the uniaxial compressive strength of sandstone samples," *Procedia Struct. Integr.*, vol. 25, no. 2019, pp. 465–469, 2020, doi: 10.1016/j.prostr.2020.04.052.

[19] R. H. Price, R. J. I. Martin, and P. J. Boyd, "Characterization of porosity in support of mechanical property analysis." 1992, Accessed: Jan. 29, 2022. [Online].Available:https://inis.iaea.org/search/search.aspx?orig_q=RN:24048088.

[20] D. C. Wyllie and N. I. Norrish, "Rock Strength Properties and their Measurement," in *Landslide: Investigation and Mitigation*, 1996, pp. 372–390.

[21] ISRM, *Rock Characterization Testing and Monitoring. ISRM Suggested Methods.* Oxford: Pergamon Press, 1981.

Citation of this Article:

Joan Atieno Onyango, Dorothy Mwanzia Kanini, Dyson Moses, Cho Thae Oo, Ulaankhuu Batsaikhan, Seelae Phaisopha, Ian Tsuma Krop, "Laboratory Investigation of the Physico-Mechanical Properties of Coral Limestone of Vipingo Area in Kenya's Coastal Region" Published in *International Research Journal of Innovations in Engineering and Technology - IRJIET*, Volume 6, Issue 2, pp 42-53, February 2022. Article DOI https://doi.org/10.47001/IRJIET/2022.602009

****

